Journal of Hydrology 616 (2023) 128780

Contents lists available at ScienceDirect

Journal of Hydrology

journal homepage: www.elsevier.com/locate/jhydrol

Research papers

Temperature effect on non-Darcian flow in low-permeability porous media

Yuntian Teng [a], Yifeng Wang [b], Zihao Li [c], Rui Qiao [d], Cheng Chen [a,*]

[a] Department of Civil, Environmental, and Ocean Engineering, Stevens Institute of Technology, Hoboken, NJ 07030, United States
[b] Sandia National Laboratories, Albuquerque, NM 87185, United States
[c] Pacific Northwest National Laboratory, Richland, WA 99354, United States
[d] Department of Mechanical Engineering, Virginia Tech, Blacksburg, VA 24061, United States

ARTICLE INFO

This manuscript was handled by Huaming Guo, Editor-in-Chief, with the assistance of Yueqing Xie, Associate Editor

Keywords:
Non-Darcian flow
Threshold pressure gradient
Temperature effect
Two-parameter model
Experiment

ABSTRACT

The Darcy's law specifies a linear relation between the Darcy velocity of a fluid flow and the pressure gradient that drives the flow. However, in low-permeability porous media, the velocity of a fluid flow exhibits a nonlinear dependence on the imposed pressure gradient, which is referred to as the non-Darcian flow behavior. Temperature has been postulated to affect the threshold pressure gradient of a non-Darcian flow; however, the supporting data is very limited due to the challenges in conducting flow experiments in low-permeability porous media. In this study we for the first time report a systematic measurement of the threshold pressure gradient under various permeabilities and temperatures. The results show that a higher temperature leads to a lower threshold pressure gradient under the same permeability and a faster reduction of the threshold pressure gradient with increasing permeability. The experimental data are fitted to a two-parameter model we previously developed to determine the parameters, h_0 and a, which characterize the interfacial fluid-solid interactions and the transition between the Darcy and non-Darcian regimes. Both h_0 and a decrease with an increasing temperature. The lower value of h_0 under a higher temperature leads to the faster decline of threshold pressure gradient with increasing permeability. This is the first comprehensive experimental study that measured the threshold pressure gradient under multiple different permeabilities and temperatures, which generated the first laboratory dataset of this kind. The experimental data and the model constrained here allow for systematic predictions of both Darcy and non-Darcian flows for a general set of low-permeability porous media under various temperatures and pressure gradients, which have important applications to geological disposal of nuclear waste, hydrocarbon extraction from shale, and contaminant remediation in clay-rich formations.

1. Introduction

The widely used Darcy's law specifies a linear relation between the Darcy velocity of a fluid flow and the pressure gradient that drives the flow (Bear, 2012). However, many studies (Miller and Low, 1963; Kutílek, 1972; Hansbo, 2001; S'anchez et al., 2007; Cui et al., 2008; Bear, 2012; Liu and Birkholzer, 2012; Liu et al., 2012) have shown that Darcy velocity can exhibit a nonlinear dependence on the pressure gradient in low-permeability porous media such as clay and shale when the pressure gradient is adequately low. This phenomenon is referred to as non-Darcian flow and is caused by strong liquid-solid interactions near solid surfaces (Miller and Low, 1963), which are due to the combined effects of various interfacial and intermolecular forces including the van der Waals forces (Liu, 2017). In low-permeability porous media, the nanoscale pore size is comparable to the interfacial layer thickness so that the influence of strong liquid-solid interactions is not negligible (Wang, 2014). In this circumstance, a threshold pressure gradient is required to overcome the resistance from the interfacial layer to trigger a fluid flow (Miller and Low, 1963; Hansbo, 2001), leading to the non-Darcian flow phenomenon.

Non-Darcian flow is a fundamental flow and transport problem, which has important implications to many natural and engineered processes in low-permeability porous media, such as geologic disposal of high-level nuclear waste, hydrocarbon energy extraction from shale formations, flow and contaminant transport in clay-rich aquifers, etc. (Hansbo, 2001; Lackner, 2003; Tsang et al., 2012; Liu, 2014; Mijic et al., 2014; Lanyon and Gaus, 2016; Zheng et al., 2020; Li et al., 2021). Particularly, in a geologic nuclear waste repository, compacted bentonite clay has been proposed as a buffer material to fill the space between the host rock and a waste container (Sellin and Leupin, 2013; Tsang et al., 2015). Advanced understanding of non-Darcian flow in a

* Corresponding author.
E-mail address: cchen6@stevens.edu (C. Chen).

https://doi.org/10.1016/j.jhydrol.2022.128780
Received 4 August 2022; Received in revised form 30 September 2022; Accepted 30 October 2022
Available online 25 November 2022

Nomenclature

a	characteristic time, s
h	thickness of immobile layer, m
h_0	thickness of static immobile layer, m
J_t	threshold pressure gradient, Pa/m
J_c	critical pressure gradient, Pa/m
k	absolute permeability, m^2
k_a	apparent permeability of the porous medium, m^2
k_p	apparent permeability of the tube, m^2
m	coefficient in the Kozeny-Carman correlation
r	distance from the tube center, m
R	tube radius, m
u	flow velocity, m/s
U	Darcy velocity through the porous medium, m/s
α	power-law exponent in the Kozeny-Carman correlation
μ	fluid viscosity, Pa•s
ϕ	porosity
$\boldsymbol{\beta}$	vector of unknown parameters in nonlinear least square fitting
$\mathbf{J}$	Jacobian matrix in nonlinear least square fitting
$\mathbf{r}$	residual vector in nonlinear least square fitting
$\frac{\partial p}{\partial x}$	pressure gradient, Pa/m

bentonite buffer is critical to an accurate prediction of water migration and the related radionuclide transport in the near field of a nuclear waste repository over a time scale of 100,000 years. Specifically, the wetting process, caused by water imbibition from the surrounding rocks to the initially dry bentonite buffer, leads to bentonite saturation and swelling, thereby increasing in-situ stress and consequently improving the sealing effect of the buffer material.

Heat generated from nuclear waste will further affect water distribution and transfer in the bentonite buffer. A recent thermal-hydrological-mechanical (THM) simulation (Rutqvist et al., 2011) showed that the temperature evolution in a bentonite-backfilled engineered barrier would range from less than 30 °C to ~90 °C over a time scale of 100,000 years. The temperature can be even higher depending on the configuration of waste emplacement. Non-Darcian flow is an important phenomenon to be considered in an overall THM modeling of a repository (Rutqvist et al., 2011, 2014). Numerous laboratory studies focused on non-Darcian flow and its dependence on hydrological and mechanical properties of the porous medium (Millard et al., 2016; Idiart et al., 2020; Zheng et al., 2020). However, our understanding of the role of temperature in such flow is very limited. Miller and Low (1963) measured the threshold pressure gradient in a clay sample under 10.15 °C and 20.00 °C and found that the threshold pressure gradient decreased with increasing temperature. Zeng et al. (2010) measured the threshold pressure gradient for oil flow in low-permeability sandstones under 70 °C and 90 °C and found a similar conclusion. Although these pioneering experimental studies provided valuable insights into the role of temperature, additional experimental data under multiple different temperatures and permeabilities are needed to unravel the underlying mechanism of the phenomenon. In addition, a theoretical framework for the interpretation of experimental data is generally missing.

In this work, we will first present a two-parameter model published previously to describe the nonlinear relationship between flow velocity and pressure gradient for a non-Darcian flow in saturated low-permeability porous media based on the consideration of interfacial liquid-solid interactions (Chen, 2019). We then report our experimental results on the measurements of the threshold pressure gradient as a function of permeability under various temperatures. The data will be fitted to the two-parameter model. Finally, the model predictions of water flux under a wide range of permeabilities, pressure gradients, and temperatures will be presented and discussed. Flow experiments in low-permeability samples are highly challenging due to the extremely slow flow velocity. Therefore, experimental data with respect to the role of temperature on non-Darcian flow is very limited in the literature. This is the first comprehensive experimental study that measured the threshold pressure gradient under multiple different permeabilities and temperatures, which generated the first laboratory dataset of this kind. The experimental data collected from this study will be valuable in the study of many hydrogeological processes such as geological disposal of nuclear waste (Liu and Birkholzer, 2012; Lanyon and Gaus, 2016; Zheng et al., 2020), hydrocarbon energy recovery (Swami et al., 2012; Dejam et al., 2017; Wang and Sheng, 2017), and flow and transport in clay-rich aquifers (Pak et al., 2020).

2. Materials and methods

2.1. Overview

Section 2.2 gives a brief description of the two-parameter model we developed in a previous study (Chen, 2019), which provides a mathematical formulation for the problem and a foundation for the fitting and interpretation of experimental data. Section 2.3 describe the laboratory equipment setup in this study, which measured the threshold pressure gradient as a function of permeability under three different temperatures. Section 2.4 describes the nonlinear least square fitting method used to fit the laboratory measurement data to the two-parameter model to determine the two parameters, h_0 and a, which aimed to provide insights into the temperature effect on non-Darcian flow.

2.2. Two-parameter model

Fig. 1A illustrates the nonlinear relationship between the flow velocity and the hydraulic pressure gradient for a non-Darcian flow in a low-permeability porous medium. In this study, the threshold pressure gradient is defined as J_t, below which no fluid flow occurs (Miller and Low, 1963; Zeng et al., 2010). J_c is referred to as the critical gradient, which is the intersection of the x axis and the extension of the linear part of the curve (Liu and Birkholzer, 2012). The definition of threshold pressure gradient (J_t) in our model is the same as other experimental studies such as Miller and Low (1963), Zeng et al. (2010), and S'anchez et al. (2007). This is because J_t is straightforward to measure in laboratory experiments if the accuracy of the equipment is sufficiently high.

In a previous paper (Chen, 2019), we developed a continuum-scale, two-parameter model to account for non-Darcian flow in water-saturated low-permeability porous media. The model hypothesizes that the porous medium is a bundle of circular tubes having the same diameter and fluid flow occurs inside the tubes. There is an immobile fluid layer at the liquid-solid interface on the inner walls of the circular tubes, which causes the threshold pressure gradient. This immobile layer thickness accounts for all combined effects that hinder fluid flow in saturated low-permeability porous media, such as strong liquid-solid interactions at solid surfaces and heterogeneity in pore size distribution. The thickness of the immobile layer, h, decreases exponentially as a function of the velocity gradient at the inner wall surface:

$$h = h_0 \exp\left(- a \frac{\partial u}{\partial r}\Big|_{r=R} \right) \quad (1)$$

where r is the distance from the tube center (m), R is the tube radius (m), h_0 is the static immobile layer thickness (m) when the flow velocity is zero, and a is characteristic time (s). h_0 and a are the two parameters in the model, and their values are determined by fitting the model to experimental data, which will be discussed later. Eq. (1) is a phenomenological correlation that aims to interpret the nonlinear relation between pressure gradient and flow velocity in saturated low-permeability porous media. For incompressible Newtonian laminar flow in a circular

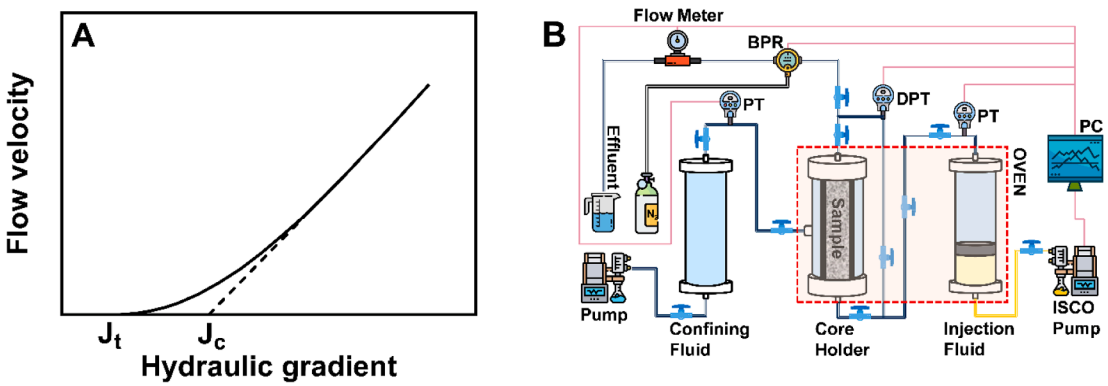

Fig. 1. A: Nonlinear relationship between flow velocity and pressure gradient for non-Darcian flow in saturated low-permeability porous media. B: Schematic diagram of the experimental setup. BPR: back pressure regulator. DPT: differential pressure transducer. PT: pressure transducer.

tube (Philip and Gerhart, 1990), the velocity gradient at the inner wall surface can be calculated as:

$$\frac{\partial u}{\partial r}\Big|_{r=R} = \frac{R}{2\mu}\left|\frac{\partial p}{\partial x}\right| \tag{2}$$

where μ is fluid viscosity (Pa·s) and $\partial p/\partial x$ is pressure gradient (Pa/m). By substituting Eq. (2) into Eq. (1), one obtains:

$$h = h_0 \exp\left(-\frac{aR}{2\mu}\left|\frac{\partial p}{\partial x}\right|\right) \tag{3}$$

When the tube radius, R, is smaller than the static immobile layer thickness, h_0, no fluid flow occurs because the entire tube is blocked by the immobile layer. A minimum (i.e., threshold) value of the absolute value of pressure gradient, $|\partial p/\partial x|$, is required to reduce h to a level smaller than R in order to trigger flow in the tube. This threshold value is the threshold pressure gradient, J_t (Pa/m). By substituting $h = R$ into the left-hand side of Eq. (3), one obtains:

$$J_t = \begin{cases} \dfrac{2\mu}{aR}\ln\left(\dfrac{h_0}{R}\right) & h_0 \geqslant R \\ 0 & h_0 < R \end{cases} \tag{4}$$

which can be written in a compact form:

$$J_t = \max\left(0, \frac{2\mu}{aR}\ln\left(\frac{h_0}{R}\right)\right) \tag{5}$$

Eq. (4) shows that $J_t = 0$ when $R > h_0$, which indicates that no threshold pressure is needed to trigger the flow. This is consistent with our experimental observation that the threshold pressure gradient vanishes or decreases to an extremely low level which is non-detectible by laboratory equipment when the absolute permeability, which is positively correlated with the pore radius, R, is higher than a certain level.

The apparent permeability of the tube is calculated as:

$$k_p = \frac{1}{8}(R-h)^2, \quad (R \geqslant h) \tag{6}$$

It should be noted that Eq. (6) is valid only when the pressure gradient is higher than the threshold pressure gradient, which leads to$R \geqslant h$, thereby enabling flow to occur in the tube. Substituting Eq. (3) into Eq. (6), one obtains the formula for calculating the apparent permeability of the tube, which is a function of the pressure gradient:

$$k_p = \frac{1}{8}\left[R - h_0 \exp\left(-\frac{aR}{2\mu}\left|\frac{\partial p}{\partial x}\right|\right)\right]^2, \quad (|\partial p/\partial x| \geqslant J_t) \tag{7}$$

where J_t is determined using Eq. (4). Eq. (7) can be substituted into the Darcy's law to calculate the Darcy velocity in the tube. It is clear that when $h_0 \geqslant R$, Eq. (7) recovers a velocity-gradient relationship where $J_c > J_t > 0$, as shown in Fig. 1A; when $h_0 < R$, $J_t = 0$ based on Eq. (4) and thus Eq. (7) reduces to the correlation of Swartzendruber (Swartzendruber, 1962), where $J_t = 0$ and $J_c > 0$; when $h_0 = 0$, Eq. (7) reduces to the classic Darcy's law, where $J_t = J_c = 0$. This indicates that, despite the simple formulation, the two-parameter model accounts for a wide variety of Darcy and non-Darcian flows in porous media. In addition, when the magnitude of pressure gradient, $|\partial p/\partial x|$, is sufficiently large, the exponential term in Eq. (7) becomes zero; in this scenario, the non-Darcian flow behavior is eliminated and thus the apparent permeability reduces to the absolute permeability, k (i.e., $R^2/8$).

Because the porous medium is modeled as a bundle of these equally-sized circular tubes, the apparent permeability of the porous medium, k_a, is calculated as:

$$k_a = \frac{\phi}{8}\left[R - h_0 \exp\left(-\frac{aR}{2\mu}\left|\frac{\partial p}{\partial x}\right|\right)\right]^2, \quad (|\partial p/\partial x| \geqslant J_t) \tag{8}$$

where ϕ is porosity, defined as the ratio of total tube cross section area (i.e., total pore area) to total sample cross section area. The Darcy velocity through the porous medium is calculated using the Darcy's law:

$$U = \frac{-k_a}{\mu}\frac{\partial p}{\partial x} \tag{9}$$

2.3. Laboratory experiments

Fig. 1B illustrates the experimental setup used in this work. The threshold pressure gradient was measured as a function of absolute permeability under 20 °C, 55 °C, and 80 °C. The sediment sample contained 10 wt% bentonite clay and 90 wt% fine sand. We mixed sand in the sample in order to accelerate the bentonite swelling process and enable the sediment structure to reach a steady state faster. The bentonite used in the experiments was the Wyoming bentonite clay, which had an average grain size smaller than 75 μm. The sand was rounded silica sand with an average grain size of 144.8 μm. The sediments were placed in a cylindrical core holder layer by layer to mitigate segregation of coarse and fine particles, and the core holder had a diameter of 25 mm and length of 60 mm. The core holder modified the confining pressure imposed on the sediments through a hydraulic pump to obtain different absolute permeabilities. We placed the core holder vertically in an oven and injected fluids from the bottom to eliminate preferential flows. The oven provided accurate temperature controls, and the injection fluid reservoir was also in the oven so that the fluid was in the equilibrium temperature. The injection fluid was a NaCl solution having ionic strength of 0.1 M, which is typical of that in natural host rocks (Bratcher et al., 2021). Because the core holder was vertically placed, the equivalent pressure gradient caused by gravity was incorporated into the total pressure gradient.

During the experiments, we first removed air from the sediment sample using a vacuum pump. We then fully saturated the sample by injecting the NaCl solution for multiple pore volumes and waited for an adequately long period of time to let clay swelling reach the steady state before the measurements. The solution was injected through the sample using a high-precision syringe pump at different flow rates. Particularly, we started from a high flow rate to eliminate the non-Darcian flow behavior. A differential pressure regulator measured the pressure difference between the two ends of the sample when the flow was in the steady state. We then reduced the injection flow rate sequentially and repeated the pressure difference measurement at each flow rate. The flow rate and pressure difference data measured within the Darcy regime were used to calculate the absolute permeability of the sample. When the flow rate decreased to an adequately low level, the flow entered the non-Darcian regime where the relationship between flow velocity and pressure gradient became nonlinear. The threshold pressure gradient, J_t, in the experiments was defined as the pressure difference normalized by the sample length when the flow rate reached 1 μL/min, which was the minimum flow rate that the syringe pump can accurately generate. When these injections were completed, we started a second round of injections from low flow rates to high flow rates. A second value of J_t was read when the flow rate increased to 1 μL/min; the average of the two values was used as the final J_t value. We conducted the second round of injections to investigate the path dependency of J_t measurements. In practice, we found that the two measured J_t values were similar, which implies that either increasing flow rates or decreasing flow rates will give the same J_t value as long as the sediments are fully saturated.

2.4. Nonlinear least square fitting

In this study, the Gauss-Newton method, an iteration-based algorithm for nonlinear least square fitting, was used to fit laboratory measurement data to the two-parameter model to determine h_0 and a. Particularly, the vector of unknown parameters, β, which has two elements in this case (i.e., h_0 and a), is calculated by:

$$\boldsymbol{\beta}^{n+1} = \boldsymbol{\beta}^{n} + \left(\boldsymbol{J}^{\mathrm{T}}\boldsymbol{J}\right)^{-1}\boldsymbol{J}^{\mathrm{T}}\boldsymbol{r} \tag{10}$$

where n indicates the iteration time step; **J** is the Jacobian matrix, in which each entry, J_{ij}, is the derivative of the model-predicted J_t value (i.e., based on Eq. (4)) with respect to the jth unknown parameter at the ith measurement; **r** is the residual vector, in which each element, r_i, is the difference between the laboratory-measured and model-predicted J_t values at the ith measurement.

3. Results and discussion

3.1. Experimental data and model fitting

Fig. 2 illustrates the laboratory-measured threshold pressure gradient as a function of absolute permeability under 20 °C, 55 °C, and 80 °C, as well as the two-parameter model fitting curves based on nonlinear least square fitting. The absolute permeability was measured within the Darcy regime where the pressure gradient was sufficiently high, the immobile layer thickness became zero, and thus the velocity depended on the pressure gradient linearly. This is the first experimental study that measured the J_t-k relationship in non-Darcian flow under multiple different temperatures. The threshold pressure gradient decreases with increasing permeability, which is consistent with other experimental studies (Lutz and Kemper, 1959; Miller and Low, 1963; Blecker, 1970; Dubin and Moulin, 1986; Zou, 1996; Cui et al., 2008; Liu and Birkholzer, 2012). Under the same permeability, a higher temperature results in a lower threshold pressure gradient, because an increased temperature would weaken the interaction energy between water molecules and clay surfaces (Miller and Low, 1963). In addition,

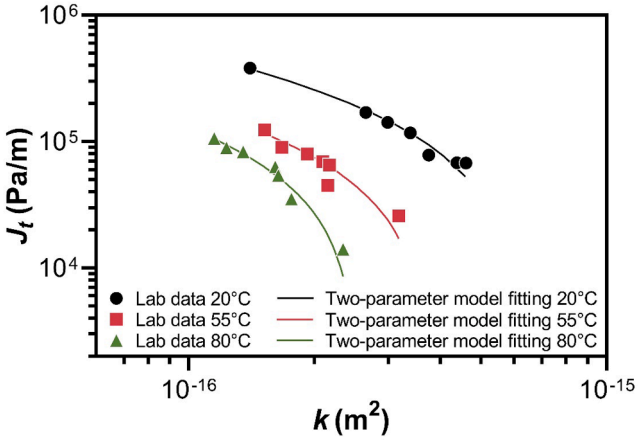

Fig. 2. Threshold pressure gradient as a function of absolute permeability under 20 °C, 55 °C, and 80 °C. The scatter data points are laboratory measurements, whereas the solid curves are obtained by fitting the measurement data to the two-parameter model using nonlinear least square fitting.

the absolute value of the slope of the J_t-k correlation increases with increasing temperature. In other words, the decline of the threshold pressure gradient with increasing permeability is faster under a higher temperature. In order to explain these observations, the variations of h_0 and a under different temperatures must be investigated to obtain mechanistic insights into the role of temperature on non-Darcian flow.

The measurement data were fitted to the two-parameter model (i.e., Eq. (4)) using nonlinear least square fitting as described in Section 2.4. Because k is the absolute permeability, R and k are related by $k = \phi R^2/8$ according to Eq. (8). In addition, k and ϕ are related based on the Kozeny-Carman correlation (Chen et al., 2016), $k = m\phi^{\alpha}$, where m is a coefficient and α is the power-law exponent. Therefore, ϕ can be written as:

$$\phi = (k/m)^{1/\alpha} \tag{11}$$

Substituting Eq. (11) into $k = \phi R^2/8$, one can calculate R as:

$$R = \sqrt{8 \cdot m^{1/\alpha} \cdot k^{(\alpha-1)/\alpha}} \tag{12}$$

Based on data fitting, we found m $= 4.0 \times 10^{-15}$ and $\alpha = 2.5$, suggesting that ϕ and k are positively correlated, which is consistent with previous studies (Chen et al., 2008, 2016). Eqs. (11) and (12) indicate that the values of ϕ and R can be determined given a particular value of k. In addition, fluid viscosity, μ, is known at a given temperature, and in Eq. (4) we use the μ value under the corresponding temperature, which suggests that the effect of temperature on fluid viscosity is accounted for in the model. Therefore, the only undetermined values in Eq. (4) are the two parameters, h_0 and a. The goal of nonlinear least square fitting was to find the optimal values of h_0 and a which gave the best fitting of the model to the laboratory measurement data.

The R^2 values of the nonlinear least square fitting were 0.991, 0.894, and 0.968 under 20 °C, 55 °C, and 80 °C, respectively, which suggests that the two-parameter model successfully fits the laboratory data, as shown in Fig. 2. Based on the fitting, the values of h_0 were found as 102.2 nm, 88.0 nm, and 78.2 nm under 20 °C, 55 °C, and 80 °C, respectively; the values of a were found as 0.037 s, 0.036 s, and 0.023 s under 20 °C, 55 °C, and 80 °C, respectively. Fig. 3 illustrates h_0 and a as a function of temperature. It is clear that both h_0 and a decreased with an increasing temperature. Particularly, the decrease of h_0 under an increasing temperature is consistent with the hypothesis in our previous study (Chen, 2019), which suggests that an increasing temperature reduces the interaction energy near solid surfaces that hinders fluid movement in low-permeability porous media. In other words, an increasing temperature reduces the static thickness of the immobile layer. In addition, the lower value of h_0 under a higher temperature

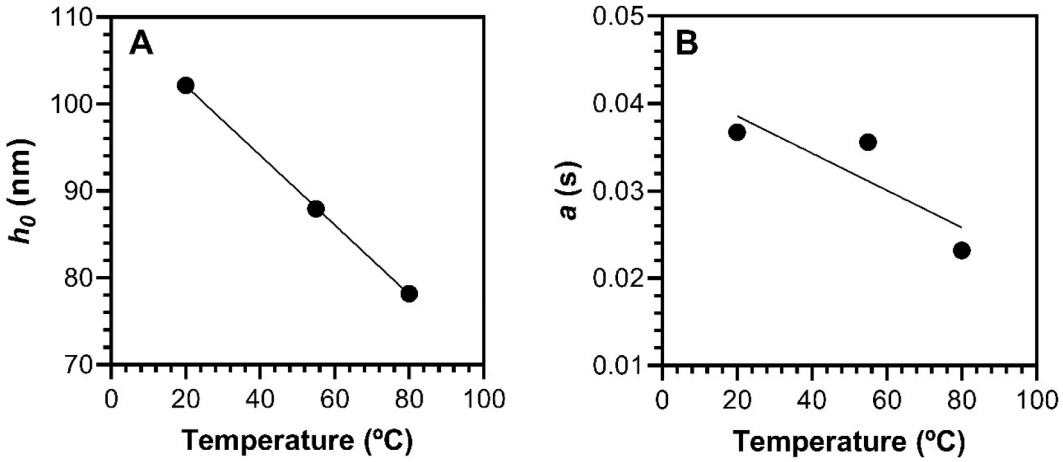

Fig. 3. A: Static immobile layer thickness, h_0, and B: characteristic time, a, as a function of temperature. The solid lines are based on linear regression fitting.

leads to the faster decline of threshold pressure gradient with increasing permeability, as demonstrated in Fig. 2. This implies that under high temperatures the threshold pressure gradient vanishes or decreases rapidly to an extremely low level that is non-detectible by laboratory equipment when the permeability exceeds a certain level, which is consistent with our laboratory observations.

3.2. Model extrapolation and prediction

The absolute permeability of an engineered clay barrier in a geological nuclear waste repository typically falls in the range between 10^{-20} m^2 and 10^{-18} m^2 (Liu, 2014; Bianchi et al., 2015). We used the fitted values of h_0 and a under 20 °C, which were obtained by fitting laboratory data in the absolute permeability range between 10^{-16} m^2 and 10^{-15} m^2, and then extrapolated the two-parameter model to an absolute permeability level as low as 10^{-20} m^2. The model-predicted threshold pressure gradient in the permeability range between 10^{-18} m^2 and 10^{-20} m^2 was between 7×10^6 Pa/m and 5×10^7 Pa/m, which was in good agreement with other experimental data (between 2.9×10^6 Pa/m and 9.9×10^7 Pa/m) (Lutz and Kemper, 1959; Miller and Low, 1963; Blecker, 1970; Dubin and Moulin, 1986; Zou, 1996; Cui et al., 2008; Xue-wu et al., 2011). This implies that in the same clay material the values of h_0 and a depend solely on temperature; when we increase the confining pressure to consolidate the clay and decrease the permeability, the same values of h_0 and a can be used in the model to predict the threshold pressure gradient for the new permeability if the temperature stays the same. Note that such a high threshold pressure gradient (i.e., 5×10^7 Pa/m) is unlikely to achieve in a repository environment, implying that an advective water flow through an engineered barrier is not possible.

In addition to extrapolation in the dimension of absolute permeability, the two-parameter model can also be extrapolated in the dimension of pressure gradient. We substituted the values of h_0 and a fitted under 20 °C into Eq. (8) to determine the apparent permeabilities under a wide range of pressure gradient magnitude, $|\partial p/\partial x|$, which was then used in the Darcy's law (i.e., Eq. (9)) to predict the flow velocities under those pressure gradients. Fig. 4A illustrates the model-predicted velocity-gradient curves under 20 °C for three different absolute permeabilities. Similarly, we used the values of h_0 and a fitted under 20 °C, 55 °C, and 80 °C to predict the velocity-gradient curves under 20 °C, 55 °C, and 80 °C, respectively, for similar absolute permeabilities, as shown in Fig. 4B. Note that the absolute permeability, k, was measured in the Darcy regime (i.e., linear section of the velocity-gradient curve), and different k values were achieved by imposing different confining pressures on the clay sample. Therefore, the absolute permeability was an output of the experimental system, rather than an input. As a consequence, it was difficult to achieve the exactly same absolute permeability among different sets of experiments due to the different responses of sample's internal pore structure to the confining pressure under different temperatures. In practice, we consider the three absolute permeabilities in Fig. 4B statistically equivalent. Fig. 4 demonstrates that Eqs. (8) and (9) successfully predicted flow velocities in the Darcy regime by comparisons with laboratory measurement data. Table 1 illustrates the model-predicted and laboratory-measured threshold pressure gradients for the five velocity-pressure gradient curves demonstrated in Fig. 4. The agreement between model predictions and laboratory measurements indicates that nonlinear least square fitting successfully minimized the difference between the two-parameter model

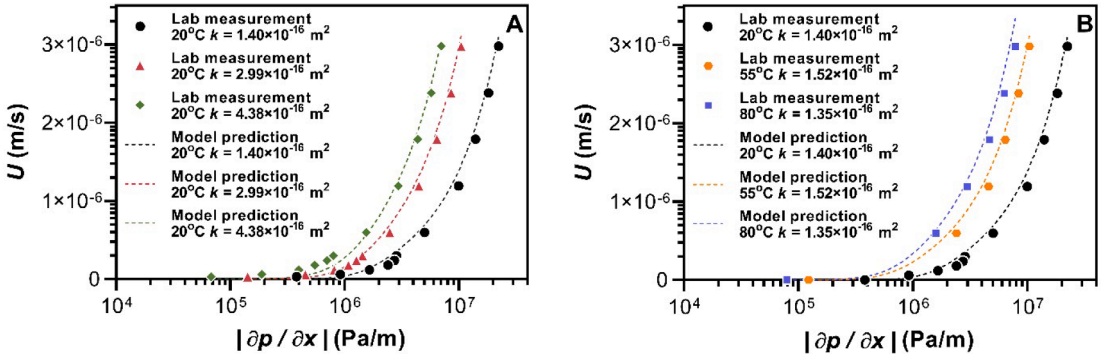

Fig. 4. A: Flow velocity as a function of pressure gradient magnitude under 20 °C for three different absolute permeabilities. B: Flow velocity as a function of pressure gradient magnitude under 20 °C, 55 °C, and 80 °C for similar absolute permeabilities. The dash lines are model predictions whereas the scatter data points are laboratory measurements.

Table 1
Model-predicted and laboratory-measured threshold pressure gradients for the experiments demonstrated in Fig. 4.

Temperature (°C)	20	20	20	55	80
Absolute permeability (m^2)	4.38×10^{-16}	2.99×10^{-16}	1.40×10^{-16}	1.52×10^{-16}	1.35×10^{-16}
Model-predicted J_t (Pa/m)	6.17×10^{4}	1.46×10^{5}	3.74×10^{5}	1.15×10^{5}	8.00×10^{4}
Lab-measured J_t (Pa/m)	6.77×10^{4}	1.42×10^{5}	3.80×10^{5}	1.23×10^{5}	8.30×10^{4}

and laboratory data, as shown in Fig. 2.

Fig. 4 illustrates the two-parameter model's extrapolation and prediction capability in the dimension of pressure gradient, which successfully describes the velocity-gradient curve in the nonlinear (i.e., non-Darcian) and linear (i.e., Darcy) regimes. Particularly, the threshold pressure gradient in the nonlinear regime determines the starting point of the curve, where flow starts to occur, whereas the linear section determines the absolute permeability. The extrapolation performance of the two-parameter model is attributed to the data fitting process which aims to determine the values of the two parameters (i.e., h_0 and a). Fig. 2 shows that we used laboratory-measured J_t and k values to fit the values of h_0 and a. Particularly, J_t determines the non-Darcian flow characteristics, whereas k determines the Darcy flow characteristics because it is the absolute permeability measured in the linear section of the velocity-gradient curve. Therefore, the fitted values of h_0 and a account for the flow properties in both the non-Darcian and Darcy regimes.

In addition, Fig. 4B demonstrates the two-parameter model's prediction capability in the dimension of temperature. It is clear that with a similar absolute permeability a higher temperature leads to a lower threshold pressure gradient. This indicates that under a higher temperature the flow enters the Darcy regime earlier with an increasing pressure gradient magnitude. In practice, the values of h_0 and a under different temperatures need to be determined using data fitting to predict the velocity-gradient curve under each particular temperature.

4. Summary, conclusions, and implications

In this work, we conducted well-controlled laboratory experiments to measure the threshold pressure gradient as a function of permeability under three different temperatures. Flow experiments in low-permeability samples are highly challenging due to the extremely slow flow velocity. Therefore, experimental data with respect to the role of temperature on non-Darcian flow is very limited in the literature. This is the first comprehensive experimental study that measured the J_t-k curve under multiple different temperatures, which generated the first laboratory dataset of this kind. The laboratory measurement data were then fitted to the two-parameter model, and the determined parameters (i.e., h_0 and a) provided mechanistic insights into the role of temperature on non-Darcian flow in saturated low-permeability porous media.

Particularly, the laboratory measurements showed that the threshold pressure gradient decreased with increasing permeability. Under the same permeability, a higher temperature resulted in a lower threshold pressure gradient. The decline of threshold pressure gradient with increasing permeability was faster under a higher temperature, which can be explained by the decreased static thickness of immobile layer (i.e., h_0) under a higher temperature. In addition, the two-parameter model has excellent extrapolation and prediction capabilities in the dimensions of absolute permeability, pressure gradient, and temperature. Specifically, the fitted values of h_0 and a in the model account for flow properties in both the Darcy and non-Darcian regimes.

The experimental data measured in this study are valuable in the fundamental study of non-Darcian flow, which has critical implications to many engineered and natural processes associated with flow in low-permeability porous media, such as geological disposal of nuclear waste, hydrocarbon energy recovery, and contaminant remediation in clay-rich formations. Future research focusing on the threshold pressure gradient in unsaturated low-permeability porous media will be necessary to further advance our understanding of this important hydrogeological phenomenon.

CRediT authorship contribution statement

Yuntian Teng: Formal analysis, Investigation, Methodology, Writing – original draft, Writing – review & editing. **Yifeng Wang:** Formal analysis, Funding acquisition, Investigation, Methodology, Writing – original draft, Writing – review & editing. **Zihao Li:** Formal analysis, Investigation, Methodology, Writing – review & editing. **Rui Qiao:** Formal analysis, Funding acquisition, Investigation, Methodology, Writing – original draft, Writing – review & editing. **Cheng Chen:** Formal analysis, Funding acquisition, Investigation, Methodology, Project administration, Resources, Supervision, Writing – original draft, Writing – review & editing.

Declaration of Competing Interest

The authors declare that they have no known competing financial interests or personal relationships that could have appeared to influence the work reported in this paper.

Data availability

Data are available through: https://doi.org/10.5281/zenodo.6338520.

Acknowledgements

The authors are thankful to the financial support provided by the U. S. Department of Energy (DOE)'s Nuclear Energy University Program (NEUP) through the Award Number of DE-NE0008806.

References

Bear, J., 2012. Hydraulics of Groundwater. Courier Corporation.
Bianchi, M., Liu, H.H., Birkholzer, J.T., 2015. Radionuclide transport behavior in a generic geological radioactive waste repository. Groundwater 53 (3), 440–451.
Blecker, R.F., 1970. Saturated Flow of Water through Clay Loam Subsoil Material of the Brolliar and Springerville Soil Series.
Bratcher, J.C., Kaszuba, J.P., Herz-Thyhsen, R.J., Dewey, J.C., 2021. Ionic strength and pH effects on water-rock interaction in an unconventional siliceous reservoir: on the use of formation water in hydraulic fracturing. Energy Fuel 35 (22), 18414–18429.
Chen, C., 2019. A continuum-scale two-parameter model for non-Darcian flow in low-permeability porous media. Hydrgeol. J. 27 (7), 2637–2643.
Chen, C., Packman, A.I., Gaillard, J.-F., 2008. Pore-scale analysis of permeability reduction resulting from colloid deposition. Geophys. Res. Lett. 35 (7), n/a–n/a.
Chen, C., Wang, Z., Majeti, D., Vrvilo, N., Warburton, T., Sarkar, V., Li, G., 2016. Optimization of lattice Boltzmann simulation with graphics-processing-unit parallel computing and the application in reservoir characterization. SPE J. 21 (04), 1425–1435.
Cui, Y.J., Tang, A.M., Loiseau, C., Delage, P., 2008. Determining the unsaturated hydraulic conductivity of a compacted sand–bentonite mixture under constant-volume and free-swell conditions. Phys. Chem. Earth Parts A/B/C 33, S462–S471.
Dejam, M., Hassanzadeh, H., Chen, Z., 2017. Pre-Darcy flow in porous media. Water Resour. Res. 53 (10), 8187–8210.
Dubin, B., Moulin, G., 1986. Influence of a Critical Gradient on the Consolidation of Clays. Consolidation of Soils: Testing and Evaluation. ASTM International, 100 Barr Harbor Drive, PO Box C700 West Conshohocken, PA 19428–2959, 354–354.
Philip, M., Gerhart, R.J.G., 1990. Fundamentals of Fluid Mechanics. Addison Wesley, New York.
Hansbo, S., 2001. Consolidation equation valid for both Darcian and non-Darcian flow. Géotechnique 51 (1), 51–54.
Idiart, A., Laviña, M., Cochepin, B., Pasteau, A., 2020. Hydro-chemo-mechanical modelling of long-term evolution of bentonite swelling. Appl. Clay Sci. 195, 105717.
Kutilek, M., 1972. Non-darcian flow of water in soils—laminar region: a review. Dev. Soil Sci. 2, 327–340.
Lackner, K.S., 2003. A guide to CO2 sequestration. Science 300 (5626), 1677–1678.
Lanyon, G., Gaus, I., 2016. Main Outcomes and Review of the FEBEX In Situ Test (GTS) and Mock-up After 15 Years of Operation. Fracture Systems Ltd.

Li, Z., Teng, Y., Fan, M., Ripepi, N., Chen, C., 2021. A novel multiphysics multiscale multiporosity shale gas transport model for geomechanics/flow coupling in steady and transient states. SPE J. 1–13.
Liu, H.-H., 2014. Non-Darcian flow in low-permeability media: key issues related to geological disposal of high-level nuclear waste in shale formations. Hydrgeol. J. 22 (7), 1525–1534.
Liu, H.-H., 2017. Fluid Flow in the Subsurface: History, Generalization and Applications of Physical Laws. Springer, Switzerland.
Liu, H.-H., Birkholzer, J., 2012. On the relationship between water flux and hydraulic gradient for unsaturated and saturated clay. J. Hydrol. 475, 242–247.
Liu, H.-H., Li, L., Birkholzer, J., 2012. Unsaturated properties for non-Darcian water flow in clay. J. Hydrol. 430–431, 173–178.
Lutz, J.F., Kemper, W.D., 1959. Intrinsic permeability of clay as affected by clay-water interaction. Soil Sci. 88 (2), 83–90.
Mijic, A., LaForce, T.C., Muggeridge, A.H., 2014. CO2 injectivity in saline aquifers: the impact of non-Darcy flow, phase miscibility, and gas compressibility. Water Resour. Res. 50 (5), 4163–4185.
Millard, A., Mokni, N., Barnichon, J.D., Thatcher, K.E., Bond, A.E., Fraser-Harris, A., Mc Dermott, C., Blaheta, R., Michalec, Z., Hasal, M., Nguyen, T.S., Nasir, O., Fedors, R., Yi, H., Kolditz, O., 2016. Comparative modelling of laboratory experiments for the hydro-mechanical behaviour of a compacted bentonite-sand mixture. Environ. Earth Sci. 75 (19), 1–18.
Miller, R.J., Low, P.F., 1963. Threshold gradient for water flow in clay systems. Soil Sci. Soc. Am. J. 27 (6), 605–609.
Pak, T., Luz, L.F.d.L., Tosco, T., Costa, G.S.R., Rosa, P.R.R., Archilha, N.L., 2020. Pore-scale investigation of the use of reactive nanoparticles for in situ remediation of contaminated groundwater source. Proc. Natl. Acad. Sci. 117 (24), 13366–13373.
Rutqvist, J., Ijiri, Y., Yamamoto, H., 2011. Implementation of the Barcelona basic model into TOUGH–FLAC for simulations of the geomechanical behavior of unsaturated soils. Comput. Geosci. 37 (6), 751–762.
Rutqvist, J., Zheng, L., Chen, F., Liu, H.-H., Birkholzer, J., 2014. Modeling of coupled thermo-hydro-mechanical processes with links to geochemistry associated with bentonite-backfilled repository tunnels in clay formations. Rock Mech. Rock Eng. 47 (1), 167–186.
S'anchez, M., Villar, M.i.V., Lloret, A., Gens, A., 2007. Analysis of the expansive clay hydration under low hydraulic gradient. In: Experimental Unsaturated Soil Mechanics. Springer, pp. 309–318.
Sellin, P., Leupin, O.X., 2013. The use of clay as an engineered barrier in radioactive-waste management – a review. Clays Clay Miner. 61 (5/6), 477–498.
Swami, V., Clarkson, C.R., Settari, A.T., 2012. Non-Darcy Flow in Shale Nanopores: Do We have a Final Answer? SPE Canadian Unconventional Resources Conference. OnePetro.
Swartzendruber, D., 1962. Modification of Darcy's law for the flow of water in soils. Soil Sci. 93 (1), 22–29.
Tsang, C.F., Barnichon, J.D., Birkholzer, J., Li, X.L., Liu, H.H., Sillen, X., 2012. Coupled thermo-hydro-mechanical processes in the near field of a high-level radioactive waste repository in clay formations. Int. J. Rock Mech. Min. Sci. 49, 31–44.
Tsang, C.F., Neretnieks, I., Tsang, Y., 2015. Hydrologic issues associated with nuclear waste repositories. Water Resour. Res. 51 (9), 6923–6972.
Wang, Y., 2014. Nanogeochemistry: nanostructures, emergent properties and their control on geochemical reactions and mass transfers. Chem. Geol. 378, 1–23.
Wang, X., Sheng, J.J., 2017. Effect of low-velocity non-Darcy flow on well production performance in shale and tight oil reservoirs. Fuel 190, 41–46.
Xue-wu, W., Zheng-ming, Y., Yu-ping, S., Xue-wei, L., 2011. Experimental and theoretical investigation of nonlinear flow in low permeability reservoir. Proc. Environ. Sci. 11, 1392–1399.
Zeng, J., Cheng, S., Kong, X., Guo, K., Wang, H., 2010. Non-Darcy flow in oil accumulation (oil displacing water) and relative permeability and oil saturation characteristics of low-permeability sandstones. Pet. Sci. 7 (1), 20–30.
Zheng, L., Xu, H., Rutqvist, J., Reagan, M., Birkholzer, J., Villar, M.V., Fernández, A.M., 2020. The hydration of bentonite buffer material revealed by modeling analysis of a long-term in situ test. Appl. Clay Sci. 185, 105360.
Zou, Y., 1996. A non-linear permeability relation depending on the activation energy of pore liquid. Géotechnique 46 (4), 769–774.